2. Treacy, M. M. J. & Newsam, J. M. *Nature* **332**, 249–251 (1988).
3. Higgins, J. B. *et al. Zeolites* **8**, 446–452 (1988).
4. Araki, T. *Z. Kristallogr.* **152**, 207–213 (1980).
5. Meier, W. M. *Pure appl. Chem.* **58**, 1323–1328 (1986).
6. Brunner, G. O. *J. Solid St. Chem.* **29**, 41–45 (1979).

The formation of controlled-porosity membranes from anodically oxidized aluminium

R. C. Furneaux, W. R. Rigby* & A. P. Davidson

Alcan International Limited, Banbury, Oxfordshire OX16 7SP, UK
* Anotec Separations Limited, Banbury, Oxfordshire OX16 7JU, UK

Synthetic membranes are used in a number of diverse applications, such as filtration[1,2], bioreactors[2,3], tissue culture[4], analytical devices including sensors[2,5], and as supports for active materials[1,5]. Narrow pore-size distribution, high pore density and thinness are often important attributes. The anodic oxidation of aluminium[6] can produce porous films possessing these features; the anodizing voltage controls the pore size and pore density, whereas the thickness is determined by the amount of charge transferred. A major problem with this technique, however, is that the films remain attached to the aluminium, with the pore base closed by an oxide barrier layer. Here we overcome this problem by progressively reducing the anodizing voltage, thereby causing perforation of the barrier layer and separation of the film as a porous membrane.

When aluminium is anodized in certain acid electrolytes, a porous oxide develops which exhibits a remarkably uniform array of cells, each containing a cylindrical pore[6] (Fig. 1*a*). During growth at constant voltage, the barrier-layer thickness remains constant because the electric field oxidizes aluminium at the metal/oxide interface and enhances chemical dissolution at the base of the pores[6–9]. A geometric model describes how the pore size and pore density are related to the barrier-layer thickness[6]. Thus, all three parameters are controlled by the voltage. Pore sizes of 10–250 nm, pore densities of 10^{12}–10^{15} m^{-2} and film thicknesses of over 100 μm can be achieved. The ability

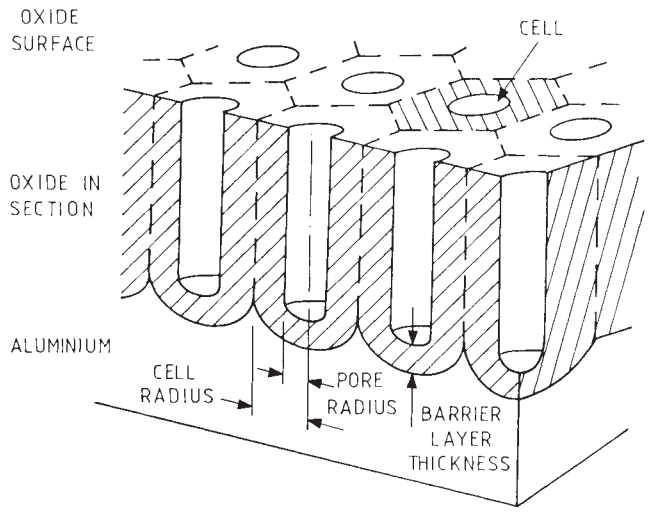

Fig. 1 Schematic diagram of a porous anodic film on aluminium, showing pores in cross-section and at a plane through the oxide, each in a hexagonal cell. During anodizing, the field is distributed across the scalloped barrier layer, separating the electrolyte within the pores from the aluminium metal.

to design porous films of pre-determined morphology makes them potentially well-suited for use as porous membranes. In order to realize this application, however, it is necessary to detach the film from the aluminium and remove the barrier layer.

The barrier-layer thickness can be reduced by lowering the anodizing voltage[6,10]. One aim of this work was to determine whether reducing the voltage to zero causes the effective elimination of a barrier layer and thus effects film separation. But when a large voltage decrement is applied in a single step, thinning occurs only at the base of few pores[10,11]. When the voltage is reduced, the field across the barrier layer becomes negligible. During the subsequent protracted induction period, chemical dissolution thins the barrier layer, probably non-uniformly from pore to pore, so that when the field begins to rise it is concentrated at only a few sites[11]. Here we describe experiments in which we decrease the voltage in a series of small steps, so as

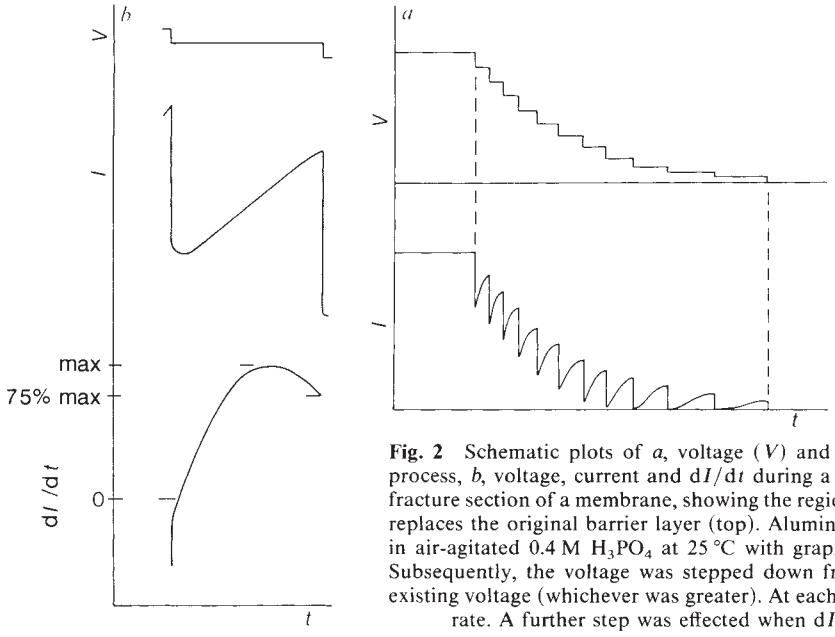

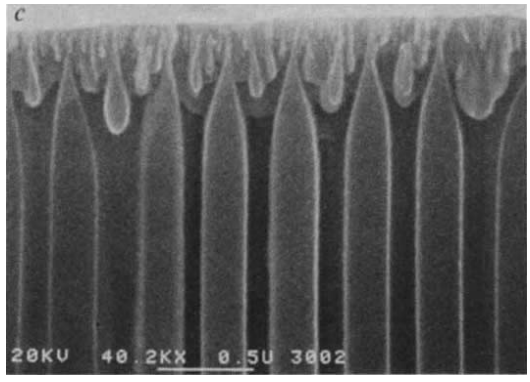

Fig. 2 Schematic plots of *a*, voltage (V) and current (I) against time during the voltage reduction process, *b*, voltage, current and dI/dt during a voltage step, and *c*, scanning electron micrograph of a fracture section of a membrane, showing the region adjacent to the surface where a divided pore structure replaces the original barrier layer (top). Aluminium (99.95% purity) was anodized at 160 V for 75 min in air-agitated 0.4 M H_3PO_4 at 25 °C with graphite counter-electrodes to produce a film 30 μm thick. Subsequently, the voltage was stepped down from 160 to 0.1 V in decrements of 0.3 V or 5% of the existing voltage (whichever was greater). At each voltage step, the current fell, and then rose at a varying rate. A further step was effected when dI/dt had fallen to 75% of its positive maximum.

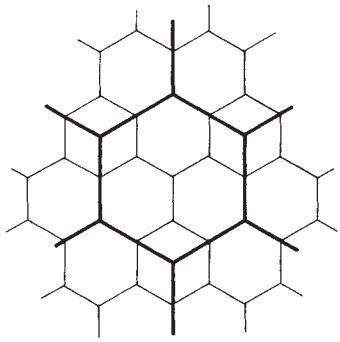

Fig. 3 Schematic representation of cell subdivision, showing how symmetry may be retained by subdivision into four.

to maintain the field at a relatively high level. It was anticipated that this would cause uniform barrier-layer thinning because, as shown by porous-film anodizing, field-assisted dissolution under high-field conditions is essentially a uniform process.

A phosphoric acid electrolyte was chosen because it permits anodization at high voltages without excessive current flow and heat evolution. Also, because they contain typically 7.5 wt% phosphate derived from the electrolyte[12], the films thus produced are relatively inert in aqueous environments[13]. The anion is distributed throughout the bulk material adjacent to the pores[14], thus determining the membrane surface chemistry. Aluminium phosphate has a particularly low solubility in aqueous solution[15], and phosphate absorbed onto alumina reduces the zero-point-of-charge from *p*H 8 to *p*H 9 (refs 16, 17). Electro-osmotic experiments[18] have shown that the membranes described here have a negative zeta potential over a *p*H range of at least 3 to 10 (D. T. Hughes and W. R. Bowen, personal communication).

Monitoring the current during the voltage-reduction process revealed short induction periods and relatively high fields (Fig. 2*a* and *b*). Electron microscopy showed that essentially every pore had divided into many smaller pores, which continued to propagate as the barrier layer thinned (Fig. 2*c*). After each voltage decrement, the current progressively rose towards the steady value associated with the new barrier-layer thickness. When the rate of current rise had fallen to 75% of its maximum value (Fig. 2*b*), a further decrement was effected. The process took about 30 min, after which penetration of the barrier layer had occurred and chemical attack at the aluminium/film interface caused detachment. The membrane had an asymmetric structure: larger pores extending through the bulk of its thickness interconnected with an array of smaller pores which formed a 'skin' at that surface originally attached to the aluminium (Fig. 2*c*).

Inspection of electron micrographs revealed that pore subdivision produces three layers of different morphology within the skin. The geometric model[6] was used to predict values for morphological parameters, which were compared with electron microscopy data of typical regions of membrane surface (Table 1 and Fig. 4). Observed values of pore size and porosity were consistently higher than those predicted, as a result of chemical dissolution in the highly acidic electrolyte. The data for the

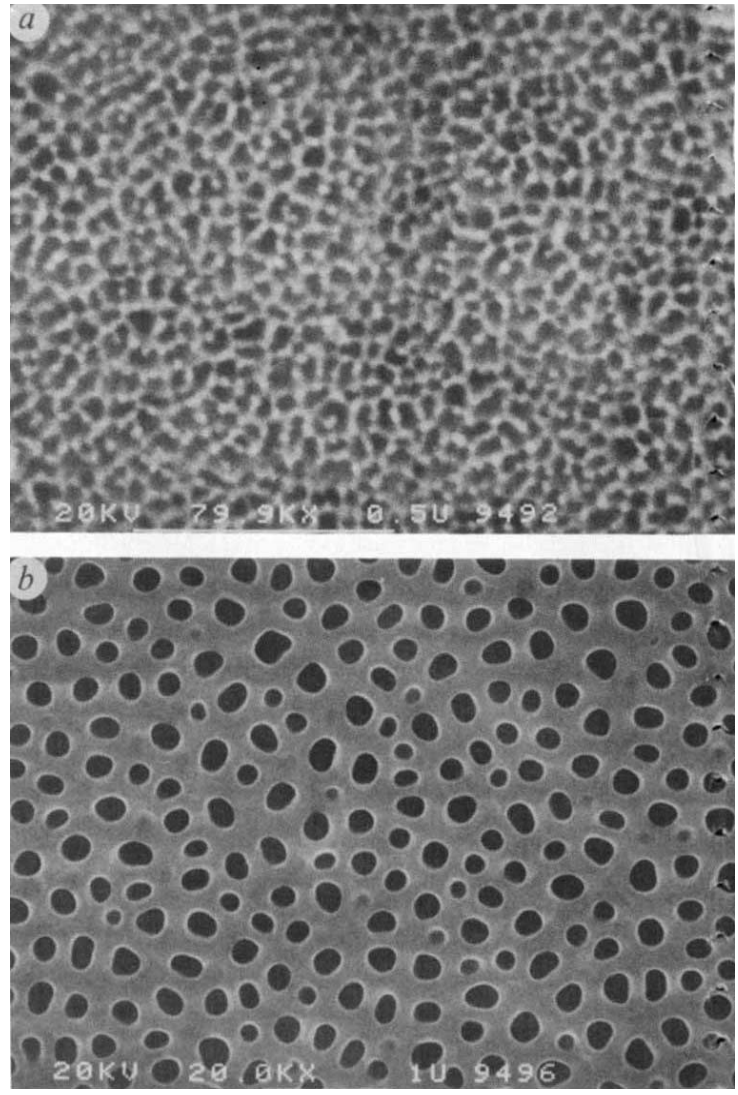

Fig. 4 Scanning electron micrographs of *a*, the surface of the membrane originally in contact with the aluminium metal, showing fine pores, and *b*, the surface of the opposite side of the membrane, after ion-beam etching, showing larger pores. Ion-beam etching (argon ions at 6 keV to 120 μA for 20 min onto the rotating membrane at 20° incidence angle) was performed to expose the steady-state pore structure below the surface, but the apparently bimodal distribution indicates that a steady-state structure was not reached.

Table 1 Comparison of theoretical and observed values for structural parameters of an anodic membrane

	Calculated			Observed		
Voltage (V)	Pore density $n_c(m^{-2})$	Pore radius p_c(nm)	Porosity P_c	Pore density $n(m^{-2})$	Pore radius p(nm)	Porosity P
160	6.8×10^{12}	80	0.14	1.1×10^{13}	80	0.25
80	2.7×10^{13}	40	0.14	—	—	—
40	1.1×10^{14}	20	0.14	—	—	—
20	4.4×10^{14}	10	0.14	3.8×10^{14}	15	0.31

The values and relationships[19] used for the calculations were: pore radius $p_c = (0.5\ \text{nm V}^{-1})V$, inscribed cell radius $c = (1.35\ \text{nm V}^{-1})V$ (p_c and c in nm), pore density $n_c = 1/\pi c^2$, porosity $P_c = (p_c/c)^2$. It was assumed that each cell, and thus each pore, divides into four to maintain symmetry, as illustrated in Fig. 3. Direct observation was achieved by electron microscopy (as shown in Fig. 4), and data were obtained from areal analysis of pore images.

ion-beam-etched surface were consistent with an original pore size of 60 nm, which is typical of a lower anodizing voltage. This reflects the initial anodizing conditions, when the voltage was increased slowly from zero. Thus it appears that the geometric model provides a valid description of anodic membranes.

We thank Mr M. C. Thornton for electron microscopy.

Received 15 September; accepted 24 September 1988.

1. Lonsdale, H. K., *J. Membrane Sci.* **10**, 81-181 (1982).
2. Michaels, A. S. & Matson, S. L. *Desalination* **53**, 231-258 (1985).
3. Flaschel, E., Wandrey, C. & Kula, M.-R. *Adv. biochem. Eng.* **26**, 73-142 (1983).
4. Vaughan, F. L., Gray, R. H. & Bernstein, I. A. *Vitro Cellular & Developmental Biology* **22**, 141-149 (1986).
5. Nylander, C. *J. Phys.* E **18**, 736-749 (1985).
6. O'Sullivan, J. P. & Wood, G. C. *Proc. R. Soc. Lond.* A**317**, 511-543 (1970).
7. Hoar, T. P. & Mott, N. F. *J. phys. Chem. Solids* **9**, 97-99 (1959).
8. Siejka, J. Ortega, C. *J. electrochem. Soc.* **124**, 883-891 (1977).
9. Thompson, G. E., Furneaux, R. C., Wood, G. C., Richardson, J. A. & Goode, J. S. *Nature* **272**, 433-435 (1978).
10. Takahashi, H., Nagayama, M., Akahori, H. & Kitahara, A., *J. Electron Microsc.* **22**, 149-157 (1973).
11. Furneaux, R. C. Thompson, G. E. & Wood, G. C. *Corros. Sci.* **18**, 853-881 (1978).
12. Alvey, C. E., Wood, G. C. & Thompson, G. E. in *Proc. 10th World Congr. Metal Finishing* (ed. Haruyama, S.) 275-280 (Metal Finishing Soc. Japan, Tokyo, 1980).
13. Thompson, G. E., Furneaux, R. C. & Wood, G. C. *Trans. Inst. Metal Finishing* **53**, 97-102 (1975).
14. Thompson, G. E., Furneaux, R. C. Wood, G. C. & Hutchings, R. *J. electrochem. Soc.* **125**, 1480-1482 (1978).
15. Vermilyea, D. A. & Vedder, W. *Trans. Faraday Soc.* **66**, 2644-2654 (1970).
16. Chen, Y.-S. R., Stumm, W. & Butler, J. N., *J. Colloid Interface Sci.* **43**, 421-436 (1973).
17. Anderson, M. A., Ferguson, J. F. & Gavis, J. *J. Colloid Interface Sci.* **54**, 391-399 (1976).
18. Bowen, W. R. & Clark, R. A. *J. Colloid Interface Sci.* **97**, 401-409 (1984).
19. Takahashi, H. & Nagayama, N. *J. chem. Soc. Japan* **36**, 34-40 (1968).

Climatic significance of δD variations in a tropical tree species from India

R. Ramesh, S. K. Bhattacharya & G. B. Pant*

Physical Research Laboratory, Ahmedabad 380009, India
* Indian Institute of Tropical Meteorology, Pune 411005, India

The climatic significance of the stable-isotope ratio of hydrogen (δD) in tree cellulose has been demonstrated using data mainly from coniferous trees that grew in temperate climates[1-4]. In such regions, the mean annual δD of precipitation is linearly related to the mean annual temperature[5], and trees thriving on precipitation preserve this temperature signal in the δD of the carbon-bound hydrogen of cellulose in their growth rings. Similar studies on tropical deciduous trees could yield useful information on climate, such as the monsoon variability over the past few centuries. However, because of the small summer-to-winter temperature contrast, tropical trees grow throughout the year and hence do not lay down well-defined growth rings (even in the few species with clear rings, it is difficult to ascertain if they are annual[6]). Also, throughout the year tropical mean surface air temperatures are >20 °C, above which the linear relation between δD of precipitation and temperature breaks down[7]. Thus there is no temperature signal in the δD of precipitation for the trees to record. In spite of these problems, we report here a significant correlation (0.7) between δD variations in two individual teak trees from the west coast of India with the amount of rainfall and mean maximum temperature, as in the case of temperate trees[4]. We propose a mechanism whereby δD of teak tree cellulose is correlated with amount of rainfall.

Teak (*Tectona grandis*, Linn. f.) was chosen because it is widely distributed in peninsular India and, unlike other tropical species, produces fairly well defined annual[8] growth rings. The timber is used extensively for a variety of construction purposes and therefore is suitable for building long tree-ring chronologies, as timber from archaeological sites may be used for this purpose. Furthermore, it grows in well drained soils[9] and therefore relies on rainwater for its growth. Several tree disks have been collected from the Murbad forest, Maharashtra, India (19°14′ N, 73°24′ E, 50 m above mean sea level). They were dated using standard procedures[10] and showed a good cross-match (similarity between ring width patterns of different trees) with no missing or double rings. The mean annual rainfall here (~60 km north-east of Bombay) is 250 cm; 95% of it falls during the monsoon season, June to September. Relative humidity ranges from 80 to 90% during monsoons and is 70% during the rest of the year. The mean annual temperature is 27.5 °C, the hottest month (May) being 6 °C hotter than the coldest (January).

Teak trees in this area remain leafless during March to May. In the first two months of monsoon (June, July), the tree starts rapid leaf growth followed by shoot growth. The cloud cover in July and August is generally 85-90% and light levels are low. Photosynthates produced during this season are used mainly for leaf expansion. The leaves grow very broad (30-60 cm across). This is followed by flowering during September and October, when the cloud cover varies from 40 to 70%. From November to February, the cloud cover is 0-2% and the temperature varies from 25 to 27 °C. Photosynthesis reaches a maximum during this period, using soil moisture stored during the later monsoon (mainly August) rains. Maximum annual ring diameter growth takes place during November to February, and is followed by some production of fruit[8,9].

Two trees, IT-2 and IT-4, that covered a span of 64 years (from 1917 to 1980 AD) were selected. The first few rings were not analysed to avoid possible juvenile effects[11]. Cellulose nitrate was prepared using standard procedures[12] from individual rings for the period 1920-1960 AD; these rings were relatively broad (2-5 mm). Subsequent rings (up to 1980) were too narrow (<1 mm) for this procedure and were analysed in groups of two to five rings. Values of δD were determined to a precision of ±2‰ using a VG Micromass 602D mass spectrometer, and the results are reported relative to the international standard V-SMOW[13].

To check the extent of intra-ring isotope variability, we analysed two radial sections of IT-4 rings corresponding to the years 1920-1954. The mean difference between the δD values was 2.8 ± 3.6‰, which was very similar to the experimental error and much smaller than the total range of variation (~30‰). The correlation coefficient between the δD values from these two sections was ~0.73. The δD values of the two trees are shown in Fig. 1*a*. The overall trends are similar and the common variance, calculated using the procedure outlined by Fritts[6], is 60%. The δD values of IT-2 are, on the whole, higher by ~10‰ than those of IT-4, possibly because of the difference in the δD of soil moisture around these trees; local differences of this magnitude in a forest are not unexpected[11], considering that the trees were separated by a distance of ~10 km.

The seasonal-rainfall-anomaly data for the Konkan meteorological subdivision (which includes the sampling site) were obtained from the records of the India Meteorological Department, Pune, and are shown in Fig. 1*b* along with the yearly mean δD values for the two trees. A positive correlation between the two is apparent. As the tree cellulose δD is also governed by climatic parameters other than rainfall, a stepwise multiple-regression analysis of the δD values, with monthly mean climatic parameters (maximum, minimum and mean temperatures, rainfall, humidity and cloudiness), was performed. This revealed that the δD of tree cellulose is significantly correlated with mean maximum temperature (T_{max}) for the period November to February and seasonal rainfall anomaly (r) for June to September:

$$\delta D = -(118 \pm 2)(0.15 \pm 0.4)r + (3.35 \pm 0.80)T_{max} \quad (1)$$

with a multiple-correlation coefficient of 0.71, significant at 0.05